remote sensing

MDPI

Article

Analysis of Factors Affecting Asynchronous RTK Positioning with GNSS Signals

Bao Shu [1], Hui Liu [1,2,*], Yanming Feng [3], Longwei Xu [1], Chuang Qian [1] and Zhixin Yang [1]

1 GNSS Research Center, Wuhan University, Wuhan 430079, China; baos613@whu.edu.cn (B.S.); lw_xu@whu.edu.cn (L.X.); qc_gnss@whu.edu.cn (C.Q.); zhixinyang@whu.edu.cn (Z.X.)
2 Collaborative Innovation Center of Geospatial Technology, Wuhan University, Wuhan 430079, China
3 Science and Engineering Faculty, Queensland University of Technology, 2 George St, Brisbane, QLD 4000, Australia; y.feng@qut.edu.au
* Correspondence: liuhui@wnlbs.com; Tel.: +86-138-0121-3637

Received: 19 April 2019; Accepted: 24 May 2019; Published: 27 May 2019

Abstract: For short baseline real-time kinematic (RTK) positioning, the atmosphere and broadcast ephemeris errors can be usually eliminated in double-differenced (DD) processing for synchronous observations. However, in the case of possible communication latency time, these errors may not be eliminated in DD treatments due to their variations during latency time. In addition, the time variation of these errors may present different characteristics among GPS, GLONASS, BDS, and GALILEO due to different satellite orbit and clock types. In this contribution, the formulas for studying the broadcast orbit and clock offset errors and atmosphere error in asynchronous RTK (ARTK) model is proposed, and comprehensive experimental analysis is performed to numerically show time variations of these errors and their impacts on RTK results from short-baselines among four systems. Compared with synchronous RTK, the degradation of position precision for ARTK can reach a few centimeters, but the accuracy degradation to a different degree by different systems. BDS and Galileo usually outperform GPS and GLONASS in ARTK due to the smaller variation of broadcast ephemeris error. The variation of broadcast orbit error is generally negligible compared with the variation of broadcast clock offset error for GPS, BDS, and Galileo. Specifically, for a month of data, the root mean square (RMS) values for the variation of broadcast ephemeris error over 15 s are 11.2, 16.9, 7.3, and 3.0 mm for GPS, GLONASS, BDS, and Galileo, respectively. The variation of ionosphere error for some satellites over 15 s can reach a few centimeters during active sessions under a normal ionosphere day. In addition, compared with other systems, BDS ARTK shows an advantage under high ionosphere activity, and such advantage may be attributed to five GEO satellites in the BDS constellation.

Keywords: relative positioning; asynchronous RTK; orbit error; clock offset error; ionosphere error; GNSS

1. Introduction

The Global Navigation Satellite System has evolved from GPS and GLONASS to four major global systems including BDS, and Galileo. The details of each system are listed in Table 1. BDS attained regional operational status Asia-Pacific in the end of 2012. Four Galileo IOV (In Orbit Validation) satellites were launched as of October 2012, 14 FOC (full operational capability) satellites have been launched by January 2018. In the last two decades, real-time kinematic (RTK) positioning has been widely used in areas such as surveying, machine automation and vehicle navigation. The GPS RTK solutions can reach the centimeter or even the millimeter level when the double-differenced (DD) carrier phase ambiguities are correctly fixed [1–3]. Given the recent development of BDS and Galileo,

GNSS systems have been widely used in RTK positioning [4–7]. Usually, these studies implicitly assume that the observations from the user and reference receiver are synchronous.

Table 1. Available satellites of each system as of January 2018.

System	Satellite Types	Satellite Number	PRN
GPS	IIR-A/B/M, IIF	32	G01-32
GLONASS	—	24	R01-24
GALILEO	IOV	4	E11,E12,E19,E20
	FOC	12	E01-05, E07-09, E22,E24,E26,E30
	ECC	2	E14, E18
BDS-II	GEO	5	C01-05
	IGSO	6	C06-C10, C13
	MEO	3	C11, C12, C14

However, for real-time positioning such as with GNSS devices on vehicles, the data from the reference receiver or network RTK server must be transmitted by wireless data link, thereby requiring transmission time to deliver the data streams of the reference receiver to the users. In addition, the reference station (or the network) may only transmit its RTCM data at a certain time interval (i.e., the update rate), which may not correspond with the data sampling rate of the user [8]. Delayed/historical reference data streams may be used along with the user data streams at the current epoch to obtain real time positioning solutions. Several studies have attempted to propose RTK solutions that may be applied in [case of data link transmission time delays. For instance, Lawrence [9] proposed the reference carrier phase prediction method, which uses past reference data to predict phase observations that are synchronized with rover data. This method obtains a reference phase prediction error of approximately 10 cm for a 10 s latency. Some rover position extrapolation techniques that use phase difference over time (PDOT) have also been proposed [10,11], where the residuals of positioning extrapolation are scaled up with the increasing number of PDOT positioning. Similar to synchronous RTK, the rover position can also be directly identified by DD positioning model for asynchronous observations. Different from synchronous RTK model, the satellite clock offset item should be considered in asynchronous RTK model [12]. Usually, this method shows a higher position accuracy compared with PDOT.

Although the variations of satellite clock offset and position during the latency time can be corrected by broadcast ephemeris, the broadcast ephemeris error may not be fully eliminated in asynchronous DD model because of the possible changes in the broadcast orbit and clock offset errors. The ionosphere and troposphere errors in the asynchronous RTK model may also be significant because of the motion of satellites during the latency time. The time variation of these errors will contaminate the asynchronous DD model and degrade the accuracy of the RTK solutions. When RTK algorithms are implemented with different systems, satellite orbit and clock types for GPS, GLONASS, BDS, and Galileo are different. The variation of broadcast orbit and clock offset, ionosphere and troposphere errors during the latency time may also show different characteristics. The impact of time delayed errors on RTK positioning among four different systems merits an investigation. In addition, understanding the characteristics of each error source for satellites in multi-GNSS systems can help optimize the stochastic model of ARTK and improve ARTK performance.

Few studies have assessed the time delay related errors in ARTK model. The variation of broadcast orbit and clock offset and ionosphere errors were simply assessed based on theoretical analysis in [12]. The assessment results were derived from empirical values according to respective error characteristics, without presenting detailed experiment analysis. In fact, these time-delay related errors are influenced by many factors, which are difficult to evaluate. The broadcast orbit and clock offset errors are related to satellite orbit type and characteristics of satellite clock hardware. The clock offset will absorb partial orbit radial error in the process of ephemeris determination [13]. In addition, the interpolation errors may be introduced when the satellite position and clock offset are calculated by interpolation

model [14,15]. Usually, the broadcast orbit and clock offset error are evaluated based on precise ephemeris [16–18]. However, smaller ephemeris error may not imply their variation during latency time being smaller. Thus, evaluating the variation of broadcast ephemeris error during specific latency time based on precise ephemeris may not be reliable. Meanwhile, the variation of atmosphere error for a special satellite is also complex; which is related to the atmosphere conditions, satellite movement and elevation angle. As a result, workable methods should be explored to evaluate the magnitude of each error source in ARTK model.

In this study, compared with synchronous RTK, the accuracy degradation of ARTK results to a different degree by different systems are presented over short baselines. To account for this, the possible factors that affect ARTK performance are assessed and compared among four GNSS systems by proposed method. First, the variation of broadcast orbit and clock offset errors during specific latency time are evaluated based on selected precise ephemeris products with one month of data. Then, the time delay related ionosphere error in the ARTK model is analyzed using various observation session data under different ionosphere conditions. Finally, some valuable findings are discussed and summarized from numerical results.

2. Methodology

The observation model and the possible error sources in ARTK model are initially introduced in this section. Afterward, the method for evaluating each error term in the model is described in detail.

2.1. Observation Model and Error Analysis for Asynchronous RTK

In the condition of time delays for the reference receiver, the historical observations from the reference receiver and the instantaneous observation of the user receiver should be used to obtain the instantaneous position of the user. We assume that the observation time for the user and reference receiver is t_1 and t_2. The un-differenced observation equation for the user is given as

$$\begin{aligned} P^j_{u,k}(t_u) &= R^j_u(t_u, t^j_u) + c \cdot [dt_u(t_u) - dt^j(t^j_u)] + \mu_k I^j_u(t_u) + T^j_u(t_u) + E^j_u(t^j_u) + \varepsilon_{P,k}(t_u) \\ L^j_{u,k}(t_u) &= R^j_u(t_u, t^j_u) + c \cdot [dt_u(t_u) - dt^j(t^j_u)] + \lambda^j_k N^j_{u,k}(t_u) - \mu_k I^j_u(t_u) + T^j_u(t_u) + E^j_u(t^j_u) + \varepsilon_{L,k}(t_u) \end{aligned} \quad (1)$$

where L and P represent the pseudorange and carrier phase observations in units of length, respectively, R is the geometric range between the satellite and receiver antenna, T denotes the troposphere error, c denotes light speed in vacuum, λ denotes the wavelength, k denotes the signal frequency number, N denotes the integer ambiguity, and μ represents the coefficient that can convert the ionosphere error on frequency 1 into frequency k with $\mu_k = f_1^2 / f_k^2$. In addition, dt^j and dt_u denote the satellite and receiver clock offset, respectively, $\varepsilon_{P,k}$ and $\varepsilon_{L,k}$ represent the observation noise of the pseudorange and carrier phase, respectively, u denotes the user receiver, j denotes a satellite, t_u denotes the true signal arriving time to the user receiver where $t_u = t_1 + dt_u$, and t^j_u represents the corresponding true signal emission time where

$$t^j_u = t_u - R^j_u / c \quad (2)$$

The geometric range R that considers the error caused by earth rotation can be expressed as

$$R^j_u(t_u, t^j_u) = \| U(t_u) r_u(t_u) - U(t^j_u) r^j(t^j_u) \| \quad (3)$$

where $U(t)$ is a coordinate transformation matrix at time t. r_u and r^j represent the position of the user and satellite, respectively. The satellite position r^j and clock offset dt^j are calculated by the broadcast ephemeris, thereby introducing the ephemeris error E (including broadcast orbit and clock offset errors).

The aforementioned description indicates that the geometric range can be seen as a variable related to signal emission and arriving time. The satellite clock offset and ephemeris error are variables related to satellite signal emission time. The other items (ionosphere error, troposphere error, and

observation noise) can be considered the variables related to signal arriving time. The code and phase hardware delay for the satellite and receiver are omitted from Equation (1) because they vary little during the short latency time and will be eliminated in double-differenced (DD) model.

The single-differenced (SD) observation between the user and reference receiver can be expressed as

$$\begin{aligned} P^j_{ru,k}(t_r,t_u) = \;& R^j_{ru}\left(t_r,t_u,t^j_r,t^j_u\right) + c\cdot\left[dt_{ru}(t_r,t_u) - dt^j\left(t^j_r,t^j_u\right)\right] \\ & +\mu_k I^j_{ru}(t_r,t_u) + T^j_{ru}(t_r,t_u) + E^j_{ru}\left(t^j_r,t^j_u\right) + \varepsilon_{P^j_{ru},k}(t_r,t_u) \\ L^j_{ru,k}(t_r,t_u) = \;& R^j_{ru}\left(t_r,t_u,t^j_r,t^j_u\right) + c\cdot\left[dt_{ru}(t_r,t_u) - dt^j\left(t^j_r,t^j_u\right)\right] + \lambda^j_k N^j_{ru,k}(t_r,t_u) \\ & -\mu_k I^j_{ru}(t_r,t_u) + T^j_{ru}(t_r,t_u) + E^j_{ru}\left(t^j_r,t^j_u\right) + \varepsilon_{L^j_{ru},k}(t_r,t_u) \end{aligned} \tag{4}$$

where t_r is the true signal arriving time to the reference receiver r where $t_r = t_2 + dt_r$, while t^j_r is the corresponding true signal emission time. The SD ephemeris error $E^j_{ru}(t^j_r, t^j_u)$ can be expressed as

$$\begin{aligned} E^j_{ru}(t^j_r,t^j_u) &= E^j_u(t^j_u) - E^j_r(t^j_r) \\ &= E^j_u(t^j_u) - E^j_u(t^j_r) + E^j_u(t^j_r) - E^j_r(t^j_r) \\ &= E^j_u(t^j_r,t^j_u) + E^j_{ru}(t^j_r) \end{aligned} \tag{5}$$

For a short baseline, the ephemeris error difference $E^j_{ru}(t^j_r)$ between the reference and user receiver at time t^j_r can be neglected because they both view the satellite in nearly the same direction. Therefore,

$$E^j_{ru}(t^j_r,t^j_u) = E^j_u(t^j_r,t^j_u) \tag{6}$$

Analogous to Equation (6), for a short baseline, the ionosphere and troposphere errors in (4) can be expressed as

$$I^j_{ru}(t_r,t_u) = I^j_u(t_r,t_u), T^j_{ru}(t_r,t_u) = T^j_u(t_r,t_u) \tag{7}$$

For short baselines, Equations (6) and (7) clearly shows the error terms in SD observation model Equation (4) when considering the observation time difference between reference and user receivers. Based on the knowledge of nature of the error terms, we make the following comments in order:

1) According to Equation (2), the signal emission time difference can be expressed as $t^j_u - t^j_r = (R^j_u - R^j_r)/c + t_u - t_r$. For short baseline, the difference in satellite-receiver geometry distance can be neglected. Thus, we have $t^j_u - t^j_r \approx t_u - t_r = t_d + dt_u - dt_r$; where $t_d = t_1 - t_2$ is the latency time. The receiver clock offset should be within ±1 ms for real-time RTCM data [19], and the value of $dt_u - dt_r$ will be within 2 ms.

2) For synchronous data, the time differences $t^j_u - t^j_r$ and $t_u - t_r$ will be both very small (within 2 ms). As a result, the variation of broadcast ephemeris error term $E^j_u(t^j_r, t^j_u)$, atmosphere error terms $I^j_u(t_r,t_u)$ and $T^j_u(t_r,t_u)$ due to 2 ms latency can usually be ignored.

3) For a few seconds of latency, the time differences $t^j_u - t^j_r$ and $t_u - t_r$ will also be a few seconds. As a result, the variation of broadcast ephemeris error term $E^j_u(t^j_r, t^j_u)$ may be significant due to the time latency. The variation of atmosphere error terms $T^j_u(t_r,t_u)$ and $I^i_u(t_r,t_u)$ due to the time latency may also be significant.

In addition, note that, the satellite clock offset term $dt^j(t^j_r, t^j_u)$ is reserved in Equation (4) after SD treatments. In general, the clock drift will be under 10^{-10} sec $/s$ level according to broadcast ephemeris data with four GNSS systems. The variation of satellite clock offset during the time difference $t^j_u - t^j_r$ are therefore negligible for synchronous data, however, it should be considered in asynchronous observation model. The clock offset item is considered for both synchronous and asynchronous data in this study.

Based on Equations (4), (6), and (7), the DD observation equation for a short baseline can be expressed as

$$\begin{aligned} P^{ij}_{ru,k}(t_r,t_u) &= R^{ij}_{ru}\left(t_r,t_u,t^j_r,t^j_u,t^i_r,t^i_u\right) - c\cdot\left[dt^j\left(t^j_r,t^j_u\right) - dt^i\left(t^i_r,t^i_u\right)\right] \\ &+\mu_k I^{ij}_u(t_r,t_u) + T^{ij}_u(t_r,t_u) + E^j_u\left(t^j_r,t^j_u\right) - E^i_u\left(t^i_r,t^i_u\right) + \varepsilon_{P^{ij}_{ru},k}(t_r,t_u) \\ L^{ij}_{ru,k}(t_r,t_u) &= R^{ij}_{ru}\left(t_r,t_u,t^j_r,t^j_u,t^i_r,t^i_u\right) - c\cdot\left[dt^j\left(t^j_r,t^j_u\right) - dt^i\left(t^i_r,t^i_u\right)\right] + \lambda^j_k N^j_{ru,k}(t_r,t_u) - \lambda^i_k N^i_{ru,k}(t_r,t_u) \\ &-\mu_k I^{ij}_u(t_r,t_u) + T^{ij}_u(t_r,t_u) + E^j_u\left(t^j_r,t^j_u\right) - E^i_u\left(t^i_r,t^i_u\right) + \varepsilon_{L^{ij}_{ru},k}(t_r,t_u) \end{aligned} \tag{8}$$

where i and j refer to reference satellite and non-reference satellite, respectively. The receiver clock offset dt_{ru} in the SD model is eliminated in the DD model because a receiver takes observations to all satellites in view simultaneously. The SD ambiguity for satellites i and j in Equation (8) can be merged into DD ambiguity for GPS, BDS, and Galileo; for GLONASS, they can form the combination of SD ambiguity and DD ambiguity, and the SD ambiguity can be calculated in advance [20]. The carrier-phase inter-frequency biases for GLONASS can be neglected for a baseline with the same receiver type [21]. After the geometric term is linearized with respect to the baseline components, the RTK observation equations, in which the baseline components and the DD ambiguities are unknown parameters for a short baseline, can be expressed as

$$E\begin{bmatrix} \delta\mathrm{P} \\ \delta\mathrm{L} \end{bmatrix} = \begin{bmatrix} \mathbf{A} & 0 \\ \mathbf{A} & \mathbf{C} \end{bmatrix}\begin{bmatrix} \mathrm{a} \\ \mathrm{b} \end{bmatrix},\ D\begin{bmatrix} \delta\mathrm{P} \\ \delta\mathrm{L} \end{bmatrix} = \begin{bmatrix} \mathbf{Q}_{PP} & 0 \\ 0 & \mathbf{Q}_{LL} \end{bmatrix} \tag{9}$$

where $E[\cdot]$ and $D[\cdot]$ denote the expectation and dispersion operators, respectively. The DD pseudorange and carrier phase residual vector δP and δL are calculated by subtracting the satellite clock offset and geometry distance from the DD pseudorange and carrier phase observations in Equation (8). a denotes the baseline vector with the corresponding coefficient matrix **A**, and b denotes the DD ambiguity vector with the corresponding coefficient matrix **C** for carrier phase observations. $\mathbf{Q}_{PP}$ and $\mathbf{Q}_{LL}$ represent the variance-covariance matrix for the pseudorange and carrier phase observations. The variance is derived following an elevation-dependent function given in [22].

By solving Equation (9) using the data from a single GNSS or Multi-GNSS, the baseline vector and float DD ambiguity vector can be determined by a Kalman filter or weighted least-squares estimation. The integer ambiguity vector is estimated by using the LAMBDA method [1]. After the ambiguity is fixed, we can obtain the fixed RTK solution.

2.2. Method for Evaluating Errors in the ARTK Model

From the above analysis, we identified that the key factors that limit ARTK performance are the variations of broadcast orbit and clock offset and atmosphere errors during the latency time. In this subsection, we give the algorithms for computing these error terms in detail.

2.2.1. Broadcast Ephemeris Error

Usually, for the GNSS positioning users, the error introduced by the broadcast orbit and clock information is called signal-in-space ranging errors (SISREs) [23]. The impact of orbit errors in the radial $_r$, along-track $_a$, and cross-track $_c$ directions on the satellite-receiver range varies with the orientation of the satellite-receiver and the user location. For a statistical description, considering the average contribution over all points of the earth within the visibility cone of the satellite is common. Refer to the papers [18,24], the orbit-only and clock-only contributions to SISREs can be expressed as a weighted average

$$\begin{aligned} SISRE_{orb} &= \sqrt{w_r^2\cdot[\mathrm{RMS}(_r)]^2 + w_{a,c}^2\cdot\left\{[\mathrm{RMS}(_a)]^2 + [\mathrm{RMS}(_c)]^2\right\}} \\ SISRE_{clk} &= \mathrm{RMS}(c\cdot_{clk}) \end{aligned} \tag{10}$$

where $_{clk}$ denote clock offset error, and the weight factors w_r and $w_{a,c}$ depend on the altitude of the GNSS satellite. The values of SISRE weight factors for four constellations have been computed as described in [16] and [17] and are provided in Table 2. When considering the influence of both clock offset error and orbit error, SISRE can be expressed as [18]

$$SISRE = \sqrt{[\mathrm{RMS}(_{r\&clk})]^2 + w_{a,c}^2 \cdot \{[\mathrm{RMS}(_a)]^2 + [\mathrm{RMS}(_c)]^2\}} \tag{11}$$

where $_{r\&clk} = w_r \cdot_r - c \cdot_{clk}$. The root-mean-square (RMS) errors in Equations (10) and (11) can be derived as

$$RMS(_P) = \sqrt{\sum_{i=1}^{N} [_P(t_i)]^2 / N} \tag{12}$$

where $P = r, a, c, clk, r\&clk$, $_P(t_i)$ denotes the orbit or clock offset error at time t_i, and N denotes the number of samples.

Table 2. Signal-in-space ranging error (SISRE) weight factors for statistical contribution of radial (R) as well as along-track (A) and cross-track (C) errors to the line-of-sight ranging error.

System	w_r	$w_{a,c}^2$
GPS	0.98	1/49
GLONASS	0.98	1/45
Galileo	0.98	1/61
BDS(MEO)	0.98	1/54
BDS(GEO, IGSO)	0.99	1/127

Based on Equation (8), the absolute broadcast ephemeris error may be not important for ARTK. For RTK using asynchronous data, we focus on the variation of broadcast ephemeris error during latency time. Analogous to Equation (11), the RMS value for broadcast ephemeris error variations during specific latency time can be expressed as

$$SISREV(t_d) = \sqrt{[\mathrm{RMS}(\Delta_{r\&clk}(t_d))]^2 + w_{a,c}^2 \cdot \left\{[\mathrm{RMS}(\Delta_a(t_d))]^2 + [\mathrm{RMS}(\Delta_c(t_d))]^2\right\}} \tag{13}$$

where $\Delta_{r\&clk}(t_d) = w_r \cdot \Delta_r(t_d) - c \cdot \Delta_{clk}(t_d)$; $\Delta_r(t_d)$, $\Delta_a(t_d)$, and $\Delta_c(t_d)$ represent the variation of radial, along-track and cross-track orbit error during latency time t_d; and $\Delta_{clk}(t_d)$ denotes the variation of clock offset error during latency time t_d. If we consider the orbit and clock offset separately, the RMS value for the specific latency variation of broadcast orbit and clock offset error can be expressed as

$$\begin{aligned} SISREV_{orb}(t_d) &= \sqrt{w_r^2 \cdot [\mathrm{RMS}(\Delta_r(t_d))]^2 + w_{a,c}^2 \cdot \left\{[\mathrm{RMS}(\Delta_a(t_d))]^2 + [\mathrm{RMS}(\Delta_c(t_d))]^2\right\}} \\ SISREV_{clk}(t_d) &= \mathrm{RMS}(c \cdot \Delta_{clk}(t_d)) \end{aligned} \tag{14}$$

Analogous to Equation (12), the RMS errors in Equations (13) and (14) can be expressed as

$$RMS(\Delta_P(t_d)) = \sqrt{\sum_{i=1}^{N} [_P(t_i, t_i + t_d)]^2 / N} \tag{15}$$

where $P = r, a, c, clk, r\&clk$, and $_P(t_i, t_i + t_d) =_P (t_i + t_d) -_P (t_i)$ denote the variation of orbit or clock offset errors between time t_i and $t_i + t_d$.

The orbit and clock offset errors of broadcast ephemeris can be calculated based on the precise ephemeris from IGS analysis centers. By taking clock offset as an example, the broadcast clock offset error at time t_i in Equation (12) can be derived as

$$\begin{aligned} {}_{clk}(t_i) &= dt_B(t_i) - dt_P(t_i) \\ &= dt_T(t_i) + {}_{clk,B}(t_i) - [dt_T(t_i) + {}_{clk,P}(t_i)] \\ &= {}_{clk,B}(t_i) - {}_{clk,P}(t_i) \end{aligned} \tag{16}$$

where dt_B and dt_P represent the clock offset calculated by broadcast and precise ephemeris, respectively. dt_T denotes the true clock offset, ${}_{clk,B}$ and ${}_{clk,P}$ denote the clock offset error of the broadcast and precise ephemeris, respectively. Generally, the precise ephemeris has a high accuracy, the value of ${}_{clk,P}$ is negligible compared with that of ${}_{clk,B}$, and ${}_{clk} \approx {}_{clk,B}$. Analogous to Equation (16), compared with precise ephemeris, the variation of broadcast clock offset error during latency time t_d in Equation (15) can be derived as

$$\begin{aligned} {}_{clk}(t_i, t_i + t_d) &= dt_B(t_i, t_i + t_d) - dt_P(t_i, t_i + t_d) \\ &= {}_{clk,B}(t_i, t_i + t_d) - {}_{clk,P}(t_i, t_i + t_d) \end{aligned} \tag{17}$$

To accurately derive the RMS value for specific latency variation of broadcast clock offset error, we must ensure that ${}_{clk,P}(t_i, t_i + t_d)$ is much less than ${}_{clk,B}(t_i, t_i + t_d)$; namely, the variation of clock offset error during latency time t_d for precise ephemeris is much less than that of the broadcast ephemeris. In this study, we should find appropriate precise ephemeris products to evaluate the variation of broadcast ephemeris error (including orbit and clock offset errors) during specific latency time.

2.2.2. Atmosphere Error

The atmosphere error in the ARTK model mainly includes ionosphere and troposphere errors. The change rate of zenith troposphere error is usually under 0.01 mm/s [25,26] and the variation of slant troposphere error will be less than 1 mm during a few seconds of latency for a satellite with 10° elevation angle. As a result, the time variation of troposphere error in ARTK processing can be neglected for short latency time. However, the variation of ionosphere error due to time latency is usually faster and larger. Under normal ionosphere activity conditions, the ionosphere variability can reach 0.4 TECU/min, i.e., approximately 1 mm/s for GPS L1 signal [27]. When accounting for mapping coefficient for satellites with low elevation angle, the ionosphere error may be significant for ARTK with a few seconds of latency. Based on Equation (1), by using the phase ionosphere residual method, ionosphere error on the L_1 signal can be calculated as

$$I^j_{u,1}(t) = \eta[L^j_{u,1}(t) - L^j_{u,2}(t)] - \eta[\lambda_1 N^j_{u,1}(t) - \lambda_2 N^j_{u,2}(t)] + \eta\varepsilon_{L_1,L_2}(t) \tag{18}$$

where $\eta = \frac{f_2^2}{f_1^2 - f_2^2}$. Assuming that no cycle slip occurs between time t and $t + t_d$, we obtain

$$I^j_{u,1}(t, t + t_d) = \eta[L^j_{u,1}(t, t + t_d) - L^j_{u,2}(t, t + t_d)] + \eta\varepsilon_{L_1,L_2}(t, t + t_d) \tag{19}$$

where t_d is the latency time, the variation of ionosphere error $I^j_{u,1}(t, t + t_d)$ during latency time can be evaluated based on this equation. The mean of the slant ionosphere error variation during specific latency time over a period of time for a satellite is obtained as follow:

$$\Delta\bar{I}^j_{u,1}(t_d) = \frac{\sum_{i=1}^{m} [I^j_{u,1}(t_i, t_i + t_d)]}{m} \tag{20}$$

where m denotes the sample size.

3. Results Analysis

In the following, we firstly present the ARTK results over short-baselines to visually show the overall impacts of time delays. Next, we examine the lumped and individual contributions of orbit and clock offset errors to ARTK model. This is followed by the analysis of the ionosphere-errors and its impact on ARTK results.

3.1. Data Collection and Processing Strategy

The data from a baseline in Perth (Australia) and a baseline in Wuhan (China) are used in this study, the longitude (Lon.) and latitude (Lat.) and other information of these two baselines are outlined in Table 3. They are very short-baselines, allowing the impact of distance dependent errors to be completely excluded. The receiver and antenna type of the rover and reference stations are consistent for these two baselines. The stations of two baselines are located on the roof of buildings, and the observation circumstance is good. The data of Baseline 1 (WHU1-WHU2) are collected from 1:00 to 1:30 on 10 January 2018. The data of Baseline 2 (CUT0-CUTA) are continuously recorded by Curtin University [28], the same three periods of data on 10 January 2018 (Day A) and 9 October 2013 (Day B) were selected for experiment analysis, respectively. The sampling rate is 1 Hz for two baselines. Day A and B represent two typical ionosphere activity days, which were under the low and high peak period of 11-year solar cycle, respectively. Table 4 lists the visible satellites for one data period from Bs.1 and six data periods from Bs.2. The cutoff elevation angle was set at 10°. The visible satellite number of three sessions on Day A from Bs.2 can satisfy positioning conditions by a single system during three selected periods for four systems. In addition, about one month (12 December 2017 to 10 January 2018) of broadcast and precise ephemeris data are collected for experiment analysis.

Table 3. General overview of two baselines. Abbreviations: longitude (Lon.) and latitude (Lat.).

Baseline	Stations	Receiver Type	Antenna	Length	Constellation	Lat. and Lon.(°)
Bs.1	WHU1-WHU2	Novatel OEM6	TRM 59800.00 SCIS	5.21 m	GPS/GLO/BDS	30.49 and 114.53
Bs.2	CUT0-CUTA	Trimble NetR9	TRM 59800.00 SCIS	8.42 m	GPS/GLO/BDS/GAL	−32.00 and 115.89

Table 4. Visible satellites during Session A1 for Bs.1 and Session A1-3, B1-3 for Bs.2.

Baseline	Session	GPS Time/Date	GPS	GLONASS	BDS	Galileo
Bs.1	A1	1:00–1:30 10 Jan. 2018	02,05,13,15,18,20, 21,24,29,30	06,07,08,09,16,20,21,22	01,02,03,04,05,06,08, 09,13,14	–
Bs.2	A1	1:00–1:30 10 Jan. 2018	02,06,12,15,19,24, 25,29,32	09,10,11,19,20,21	01,02,03,04,05,07,08, 09,10,11,13	02,03,08,11,12,14,24
Bs.2	A2	6:30–7:00 10 Jan. 2018	10,15,16,18,20,21, 25,26,27,29,31	01,07,08,12,13,14,22,23,24	01,02,03,04,05,06,07, 08,10,13	02,03,05,09,14
Bs.2	A3	14:30–15:00 10 Jan. 2018	01,03,06,07,09,11, 17,19,22,23,31	03,04,05,13,14,15,18,19,20	01,02,03,04,05,06,07, 08,09,12,13	02,07,08,18,26
Bs.2	B1	1:00–1:30 9 Oct. 2013	01,04,07,11,13,17, 20,23,31,32	04,05,06,14,15,16,19,20,21	01,02,03,04,05,06,07, 09,10	–
Bs.2	B2	6:30–7:00 9 Oct. 2013	05,07,08,09,10,13, 15,17,26,28	01,07,08,09,10,11,19,20	01,02,03,04,05,06,07, 08,09,10	–
Bs.2	B3	14:30–15:00 9. Oct. 2013	05,12,21,25,29,31	01,08,13,14,15,17,23,24	01,02,03,04,05,06,07, 08,10,11,12	–

In this study, the setting of the simulated latency time for asynchronous reference data is illustrated by Figure 1, where the latency time varies from 0 s to 14 s, then remains at 15 s latency for 45 s. This setting is repeated every minute. The synchronous data (zero-latency) is processed first to obtain corrected integers, if there is no cycle slip, which are then kept fixed in asynchronous data processing for position solutions. Both synchronous and asynchronous data are processed with the same ARTK model in Equation (9). All the data were processed by self-developed software in post-processing mode.

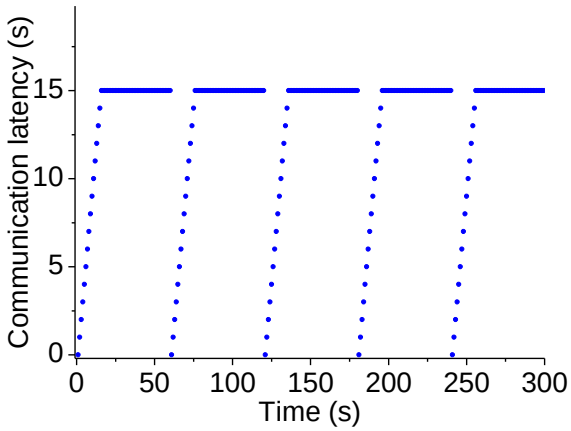

Figure 1. Simulated latency time for asynchronous real-time kinematic (ARTK)

3.2. Impact of Time Delays on RTK Results over Short-Baselines

Using the broadcast ephemeris and all available dual-frequency data, Figures 2 and 3 compare the position errors of synchronous and asynchronous RTK solutions for session A1 from two baselines, respectively. Table 5 shows the position RMS values of both RTK solutions obtained with data sets from individual systems over the two baselines. Although the signal types are different for GPS, GLONASS, BDS, and Galileo, the synchronous RTK performance for four systems are of little difference over short baselines. The horizontal and vertical RMS values from synchronous RTK processing are within 5 mm from each system in both baselines. When the processing is switched to the asynchronous data, the position accuracy is degraded to a few centimeters, but the RMS results show different degrees of accuracy degradation from different systems. For two baselines at different places, it appears that BDS are more resilient to the problems of asynchronous data sets than GPS and GLONASS are. Although the Galileo satellite number is fewer, however, Galileo ARTK also shows higher precision than those of GPS and GLONASS ARTK for Bs.2. The accuracy degradation in ARTK may be attributed to the variation of broadcast ephemeris and ionosphere errors during latency time, further analysis is conducted in the next subsection to reveal possible causes by broadcast ephemeris errors on ARTK performance among the four systems.

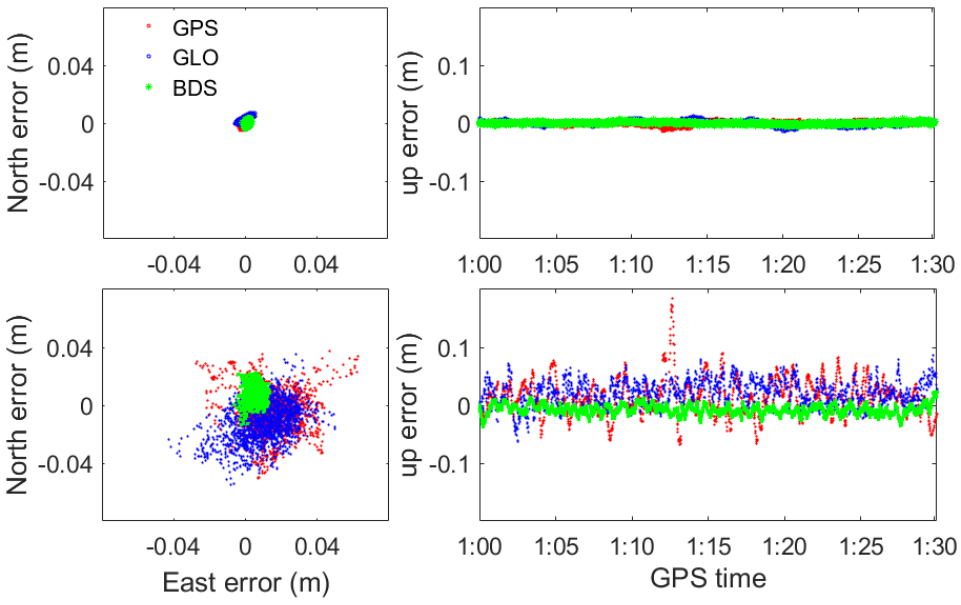

Figure 2. Real-time kinematic (RTK) position errors resulting from synchronous (**top**) and asynchronous (**bottom**) data in Session A1 for Bs.1.

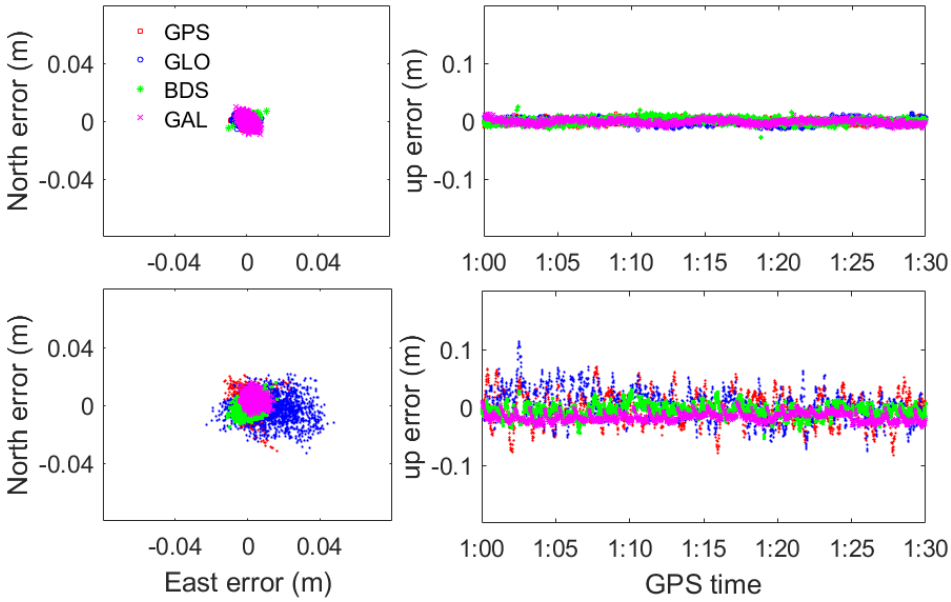

Figure 3. RTK position errors resulting from synchronous (**top**) and asynchronous (**bottom**) data in Session A1 for Bs.2.

Table 5. The root mean square (RMS) errors (mm) of SRTK and ARTK solutions for Bs.1 and 2.

		GPS			GLONASS			BDS			Galileo		
		E	**N**	**U**	**E**	**N**	**U**	**E**	**N**	**U**	**E**	**N**	**U**
Bs.1	SRTK	1	1	3	2	2	4	1	1	3	-	-	-
	ARTK	19	15	35	16	17	30	6	10	12	-	-	-
Bs. 2	SRTK	2	2	4	3	2	5	3	2	5	3	3	5
	ARTK	6	7	27	17	9	26	4	5	12	5	6	18

3.3. Broadcast Orbit and Clock Offset Error Analysis

As revealed in the Methodology section, a prerequisite in evaluating broadcast ephemeris error in the ARTK model is to identify an appropriate precise ephemeris. To find which set of orbit products suits the best for the purpose of assessment of broadcast ephemeris error variation, we directly compare ARTK positioning error statistics using these products. A smaller ARTK position error corresponds to a smaller variation of ephemeris error. We acknowledge that the GPS precise ephemeris from the IGS analysis center is most abundant, and we take GPS as an example. There are seven types of precise GPS orbit and clock products available for the International GNSS services (IGS) data centers, including the IGS ultra-rapid (igu-15 min), rapid (igr-5 min), and final (igs-5 min) ephemeris and precise ephemeris from GFZ (gbm-30 s), CODE (cod-30s and cod-5s), and CNES (c2t-5 s). The time in brackets are the sample interval of precise clock offset products, the sample interval of orbit product for all precise ephemeris is 15 min. For all precise ephemeris, the orbit and clock offset are interpolated by polynomial and linear model, respectively. Figure 4 shows the position RMS values of GPS ARTK using seven precise ephemeris for Bs.2 (the same observation session as Section 3.1). The results indicate that both cod_5s and c2t-5s products provide more desirable ARTK positioning results.

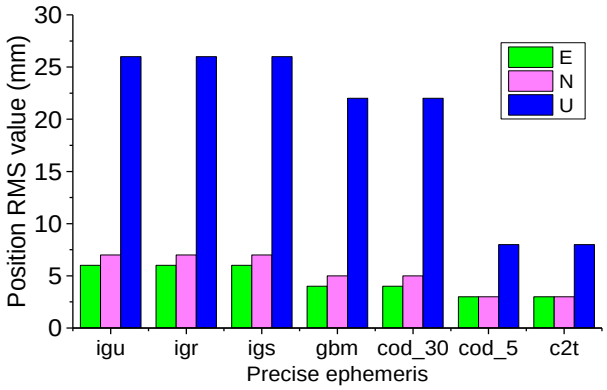

Figure 4. Position RMS value of GPS ARTK using different precise ephemeris for Bs.2.

The cod-5s final precise ephemeris from CODE only includes GPS and GLONASS, a precise ephemeris that includes four systems is required in this study. As a result, CNES's c2t-5s products with four systems are then chosen to compute the further analysis. Figure 5 presents L1 carrier residuals for GPS ARTK using the broadcast and c2t-5s ephemeris. The SD residuals are derived with the fixed coordinate parameters [29]. It is clearly seen that the amplitude and magnitude of the residuals using c2t ephemeris is obviously smaller relative to that derived from the broadcast ephemeris.

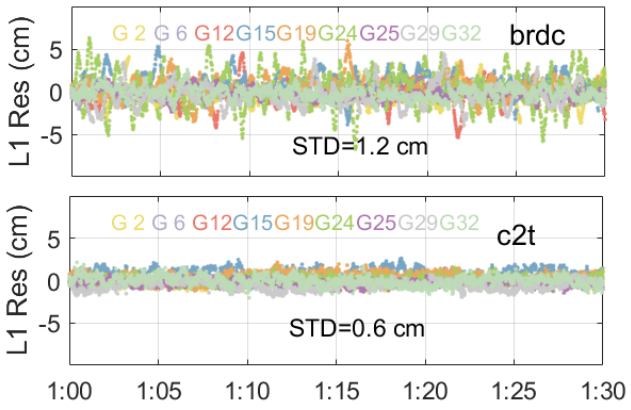

Figure 5. Illustration of L1 carrier residuals for GPS ARTK using broadcast and c2t-5s ephemeris.

Using the c2t orbits and clocks, the RMS results for the broadcast orbit and clock offset errors with different latency time internal can be calculated from the Equation (14). Figures 6 and 7 illustrate the RMS results for the broadcast orbit and clock offset errors over the varying latency of 1, 5, 10, and 15 s using 24-h span ephemeris data. The average RMS statistics of broadcast orbit error variation over the latency of 15 s are 1.6, 9.3, 2.6, and 1.4 mm for GPS, GLONASS, BDS, and Galileo. The variation degree of GLONASS broadcast orbit errors is obviously larger than that of GPS, Galileo and BDS. The average RMS statistics for the variation of broadcast clock offset error over the latency of 15 s are 10.6, 14.0, 6.3, and 2.6 mm for GPS, GLONASS, BDS, and Galileo, respectively. Compared with the influence of orbit error, the clock offset error influence appears more dominating for the ARTK model. The variation of clock offset error for GPS and GLONASS is higher than BDS and Galileo. Galileo outperform for both orbit and clock offset all other systems. Furthermore, Figure 7 shows that the RMS statistics of broadcast clock offset error variation for GPS satellites G01, G03, G06, G09, G10, G25, G26, G27, G30, and G32 are obviously smaller than those of other GPS satellites. They are Block IIF satellites by January 10, 2018. These ten Block IIF satellites are loaded with Rubidium (Rb) clocks, the other two Block IIF satellite (G08, G24) are loaded with Cesium (Cs) clocks [30]. In addition, the RMS results for the broadcast orbit and clock offset errors indeed grow with the latency time being increased from 1, to 5, 10, and 15 s.

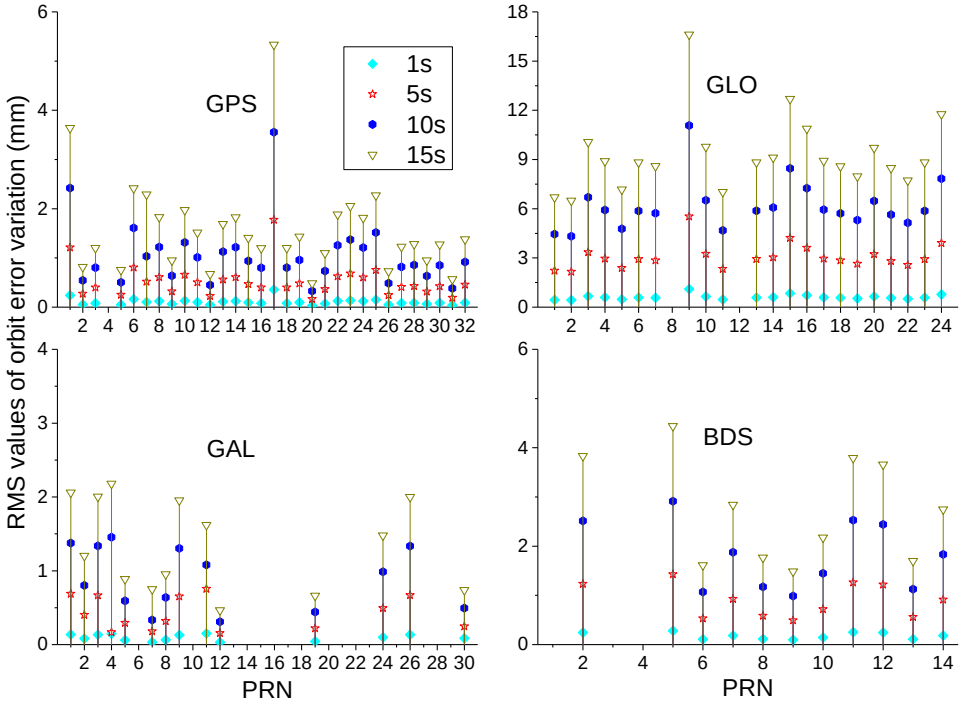

Figure 6. RMS result for 1, 5, 10, and 15 s latency variation of broadcast orbit error on 10 January 2018.

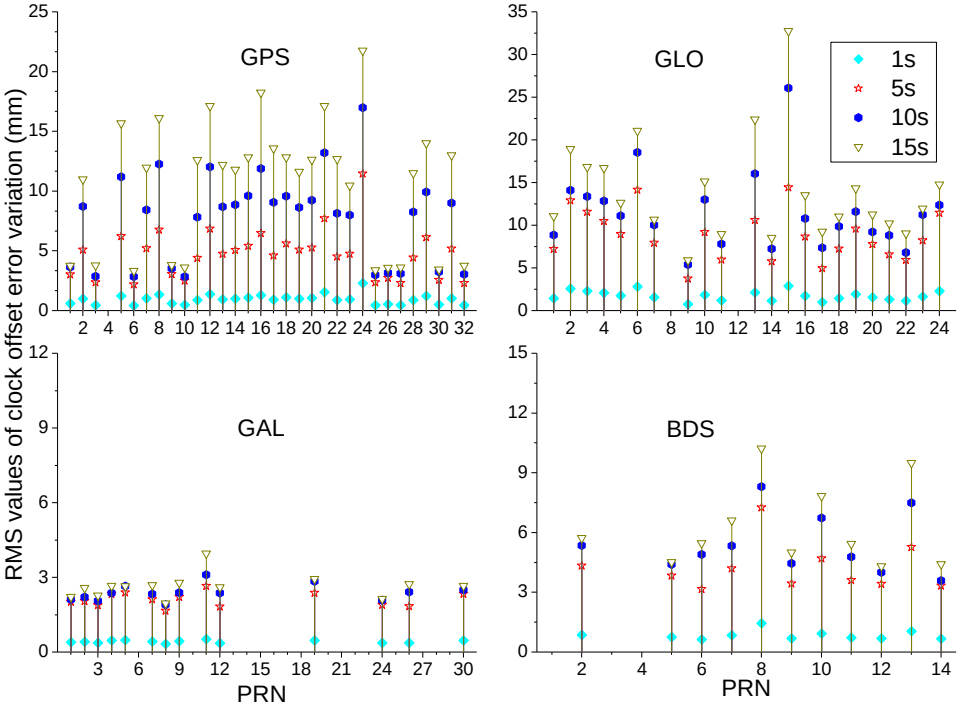

Figure 7. RMS result for 1, 5, 10, and 15 s latency variation of broadcast clock offset error on 10 January 2018.

Using Equation (13), the RMS result for the variation of the total broadcast orbit and clock error is also calculated using 24-h span ephemeris data. Figure 8 shows RMS result for 1, 5, 10, and 15 s latency variation of broadcast ephemeris error. The average RMS values for 15 s latency variation of broadcast ephemeris error are 10.8, 17.0, 7.3, and 3.1 mm for GPS, GLONASS, BDS, and Galileo, respectively. For the same time latency, the RMS result of broadcast ephemeris error variation is close to that of broadcast clock offset error variation for GPS, BDS, and Galileo. For GLONASS, the RMS value of orbit error

variation is larger, but the variation of broadcast ephemeris error remains predominately influenced by clock offset error variation. To show the consistence of RMS results for broadcast ephemeris error variation. Figure 9 shows the RMS results for 15 s latency broadcast ephemeris error from four different days. Table 6 summarizes the average RMS result for 1, 5, 10, and 15 s latency variation of broadcast ephemeris error for a period from 12 December 2017 to January 10, 2018. The average RMS result for 15 s latency variation of broadcast ephemeris error is 11.2 mm (4.3 mm for aforementioned 10 Block IIF satellites, 14.4 mm for the other GPS satellites) for GPS, where the values is 16.9, 7.3, and 3.0 mm for GLONASS, BDS, and Galileo, respectively. For certain latency time, the variation of broadcast ephemeris error for GPS and GLONASS is higher that of BDS and Galileo. This may be the reasons for the smaller ARTK position errors with BDS and Galileo.

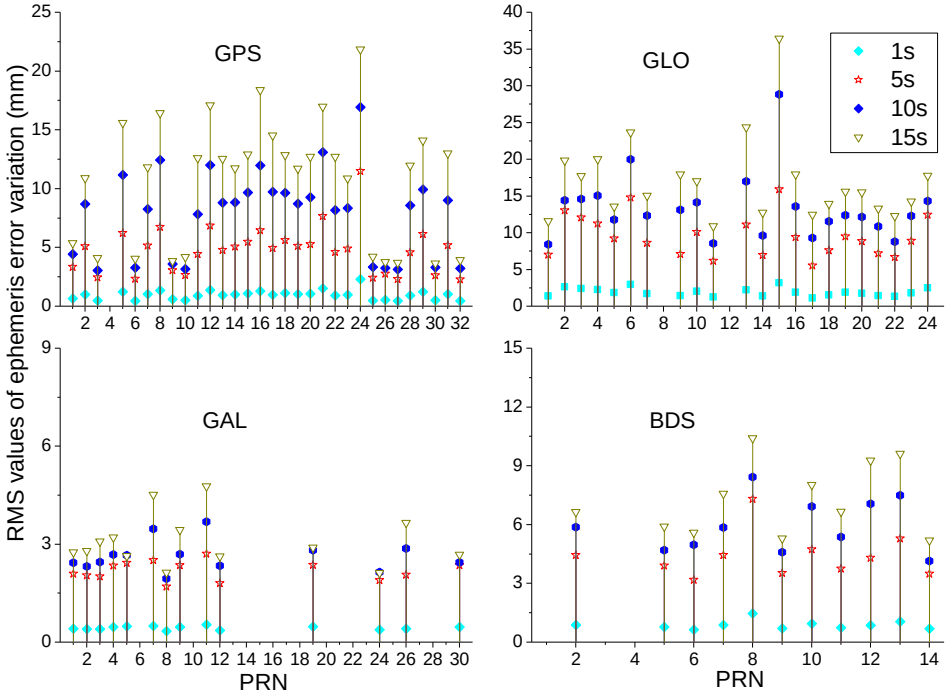

Figure 8. RMS result for 1, 5, 10, and 15 s latency variation of broadcast ephemeris error on 10 January 2018.

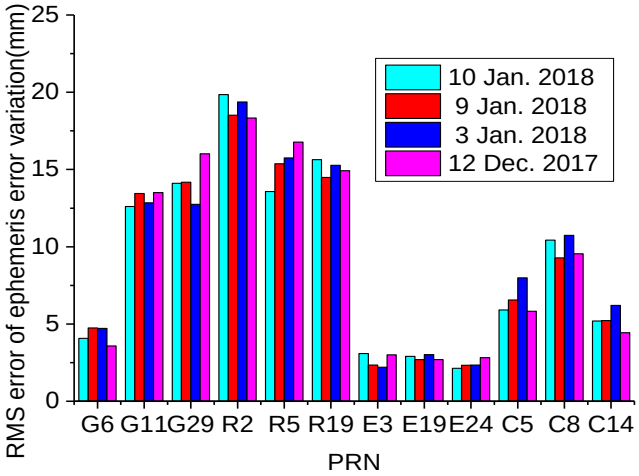

Figure 9. RMS result for 15 s latency variation of broadcast ephemeris error in four different days.

Table 6. Average RMS result (mm) for 1, 5, 10, and 15 s latency variation of broadcast ephemeris error obtained over a month (from 12 December 2017 to 10 January 2018).

Latency Time	GPS (Ten Block IIF)	GPS (Other Satellites)	GLONASS	BDS	Galileo
1s	0.5	1.2	1.9	0.4	0.9
5s	2.6	5.8	9.5	2.2	1.4
10s	3.4	10.0	13.3	5.9	2.6
15s	4.3	14.4	16.9	7.3	3.0

3.4. Ionosphere Error Analysis

Apart from the ephemeris error, the ionosphere error in the ARTK model is also analyzed. Together with the data of Session A1 from Bs.2, the effects of ionosphere error term in ARTK model are now more specifically examined with the data of another five sessions (Sessions A2-3, B1-3). The local time at Perth (Perth time) is 8 h earlier than the GPS time. Generally, Sessions A1-3 or B1-3 represent three different ionospheric activity levels in one day. The ionospheric activity level in the early afternoon (Sessions A2, B2) is most serious, the ionospheric activity level in the morning (Sessions A1, B1) is medium and in the middle night (Sessions A3, B3) is relatively low.

Figure 10 shows ARTK position errors of Sessions A2-3 from Bs.2 when the broadcast ephemeris is used. Table 7 shows the RMS error of ARTK for Sessions A1-3, B1-3 using broadcast and precise ephemeris (c2t), there were no 5-s interval precise clocks for BDS in 2013. The same as Session A1, the results from all sessions show that BDS has a better ARTK performance compared with GPS and GLONASS when the broadcast ephemeris is used. Galileo ARTK performs well in Session A3, but the precision obviously decreases in Session A2. The serious performance decreases of Galileo ARTK in Session A2 is attributed to worse geometry structure, only five satellites were observed, showing less resilient to the variation of ionosphere errors than all other systems. Table 7, a comparison of the results using broadcast ephemeris with a precise ephemeris, shows that the GPS and GLONASS ARTK performance is improved, whereas the performance of BDS and Galileo ARTK using precise ephemeris is a little worse than that using broadcast ephemeris for three sessions on January 10, 2018. The main reason for the worse performance with BDS and Galileo RTK is that the real-time c2t ephemeris is not as stable as final precise ephemeris. Particularly for three visible BDS satellites C01, C03, and C04, their precise ephemeris are unavailable in A1-3. In Galileo constellation, the E14 precise ephemeris are unavailable during Sessions A1-2, and the E18 precise ephemerides are unavailable during Session A3. As a result, the ARTK satellite geometry in the ARTK model worsens due to fewer observations. But we can still observe that the ARTK performance is more significantly degraded under active ionosphere conditions.

To show the influence of ionosphere error variation on ARTK model clearly, Figure 11 shows the RMS result for carrier residuals on L1 signals for GPS, GLONASS, BDS, and Galileo ARTK using broadcast and c2t ephemeris. The residuals are derived with the fixed coordinate parameters. When the precise c2t ephemeris is used, the carrier residuals are mainly influenced by the ionosphere error variation due to latency time. In consistence with the ionosphere activity level, the L1 carrier residuals during Session A2/B2 are generally higher than those from Sessions A1/B1 and A3/B3. The L1 carrier residuals for the data collected on 9 October 2013 are higher than that collected on 10 January 2018.

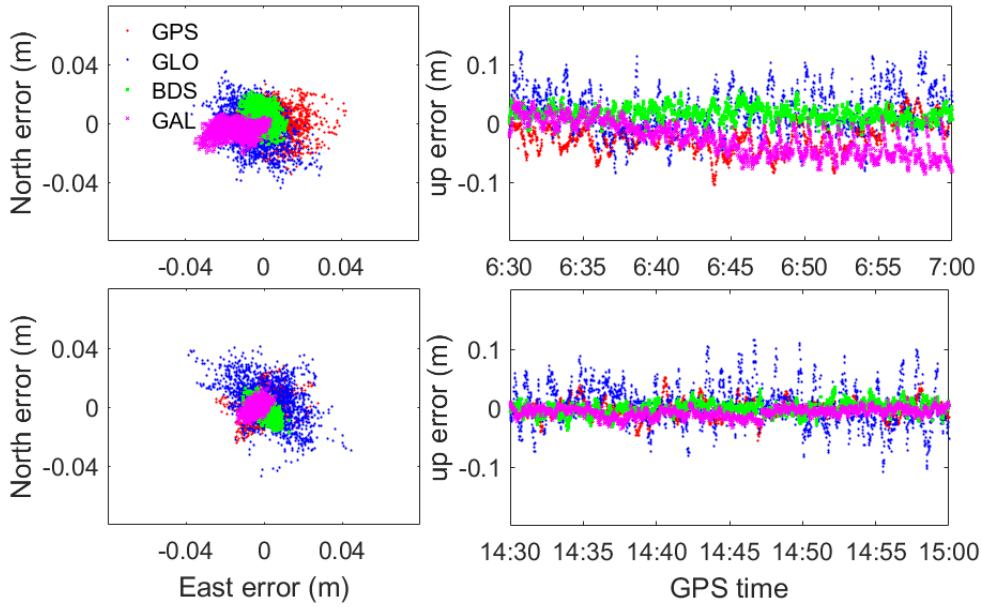

Figure 10. ARTK position errors of Sessions A2 (**top**) and A3 (**bottom**) for Bs.2.

Table 7. ARTK position RMS (mm) of Sessions A1-3, B1-3 from Bs.2 using broadcast and c2t ephemeris.

Session		GPS			GLONASS			BDS			Galileo		
		E	N	U	E	N	U	E	N	U	E	N	U
A1	brdc	6	7	27	17	9	26	4	5	12	5	6	18
	c2t	4	3	8	13	6	10	5	5	13	5	6	21
A2	brdc	11	10	34	11	13	42	4	7	19	18	6	39
	c2t	7	7	29	5	16	36	12	11	34	28	8	46
A3	brdc	7	7	15	12	14	35	3	5	10	5	4	12
	c2t	3	4	6	5	5	15	6	4	9	6	5	13
B1	brdc	12	18	20	10	8	51	4	5	16	—	—	—
	c2t	11	16	18	6	6	41	—	—	—	—	—	—
B2	brdc	12	12	24	20	16	47	6	12	16	—	—	—
	c2t	6	11	14	14	14	46	—	—	—	—	—	—
B3	brdc	11	16	32	13	13	30	3	6	14	—	—	—
	c2t	5	6	12	7	4	16	—	—	—	—	—	—

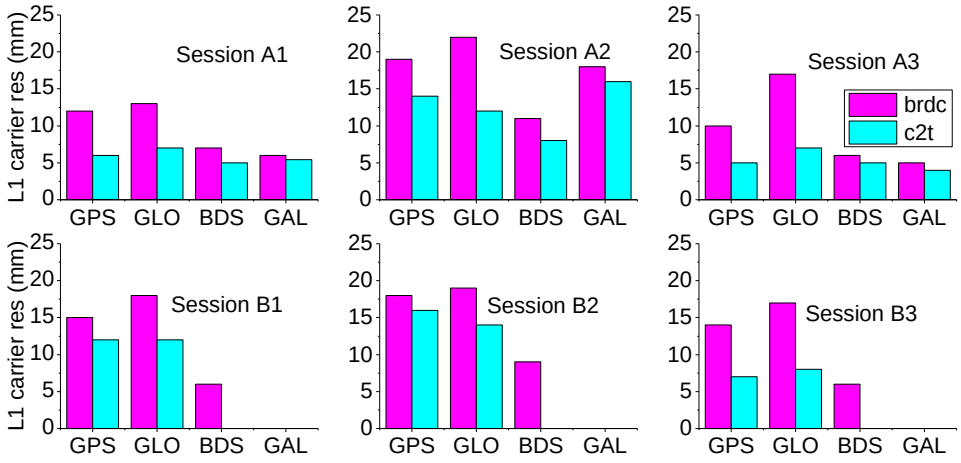

Figure 11. L1 carrier residuals for GPS, GLONASS, BDS, and Galileo ARTK using broadcast, c2t ephemeris.

Comparing the L1 carrier residuals for four different systems in Figure 11, we can also see that the L1 carrier residuals for BDS are smaller than that of GPS and GLONASS when the broadcast ephemeris is used. This may be attributed to relatively small variation of broadcast ephemeris error for BDS. When the ephemeris errors for GPS and GLONASS (using c2t ephemeris) are remarkably reduced, the L1 carrier residuals of BDS remain smaller than those of GPS and GLONASS in Sessions A2, B1, and B2. Generally speaking, the ionosphere activities in these sessions are relatively active. This implies that BDS ARTK shows an advantage under higher ionosphere activity. Figure 12 illustrates the average 15 s latency variation of slant ionosphere error during Session 2 for every visible satellite with dual-frequency signals according to Equation (20). The average elevation angle and its average change rate are also plotted. By averaging, the effects of measurement noise in the ionosphere error variation determined by Equation (20) becomes very small. The GLONASS satellites R12 and R24 are not illustrated because only L1 frequency signals are collected. Figure 12 shows that the variation of ionosphere errors is as large as several centimeters, when the satellite elevation angle is low and its change rate is rapid, including: 3.8 cm (G25), 2.8 cm (G31), 4.6 cm (R01), 2.7 cm (E02), and 2.2 cm (E03). The 15 s latency variation of ionosphere errors for some satellites are very small: 0.3 cm (G15), 0.1 cm (C05), and 0.02 cm (E09), although their satellite elevation angles are under 20°. It is noted that the elevation angle change rate of these satellites is slow during this session. For BDS, 5 visible GEO satellites are observed in their coverage area. The geometry stays almost unchanged, and the ionosphere influence on ARTK results is small with these satellites, despite the ionosphere activity level being relatively high.

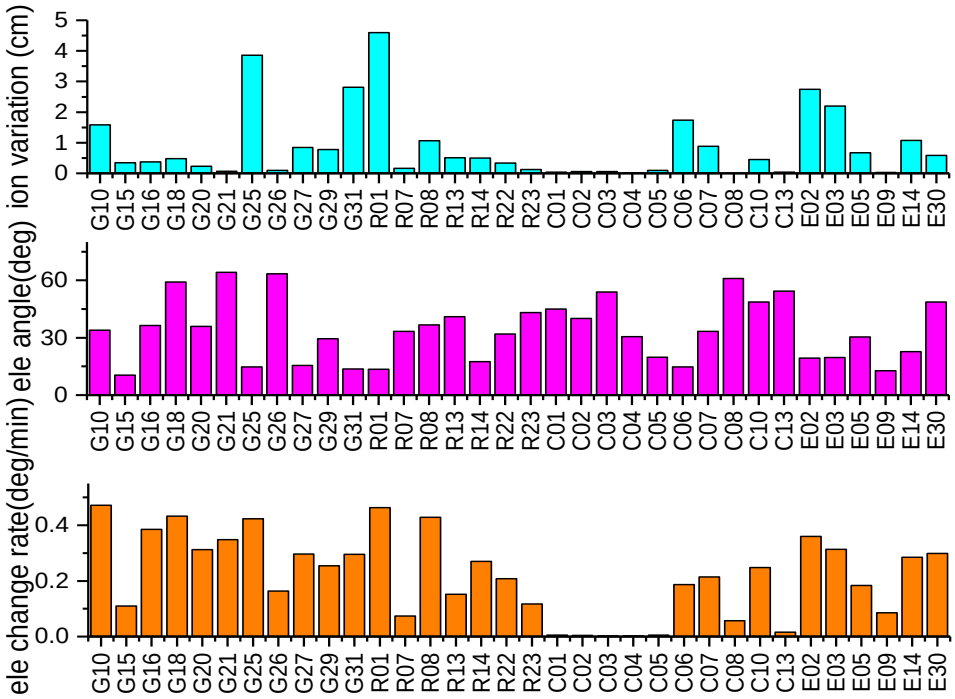

Figure 12. Average 15 s latency variation of ionosphere error (top), elevation angle (middle), and the change rate of elevation angle (bottom) in Session A2.

4. Discussion

Compared with position RMS error of ARTK using broadcast ephemeris (6, 7, and 27 mm, Table 5), no obvious improvement was observed for ARTK using igu, igr, and igs ephemeris in Figure 4. As we known, the precision of IGS final ephemeris is higher than IGS ultra-rapid and rapid and broadcast ephemeris, thereby possibly introducing confusion that ARTK positioning result is almost the same. Meanwhile, from Figure 4, it is observed that using the IGS final ephemeris products igs-5min results in higher RTK uncertainty than using cod-5s and c2t-5s products. In fact, the interpolation model is used

to calculate the satellite position and clock offset by broadcast ephemeris and precise ephemeris, which will be introduced interpolation errors. Similar to the results of clock offset extrapolation [31,32], it is expected that the shorter the interpolation time span, more accurate the interpolation model will be. The interpolation time span is related to the interval of ephemeris products. Therefore, the interpolation errors from igs-5min and igu-15min ephemeris will be smaller than that from 2-h broadcast ephemeris. And the interpolation errors from cod-5s and c2t-5s ephemeris will be smaller than that from igs-5min ephemeris. The smaller interpolation errors may not imply the variation of interpolation errors during short latency time being smaller, but the variation of interpolation errors during short latency time tends to be smaller when the interpolation model is precise enough (such as 5-interval interpolation model) to represent the detailed variations of clock offset information. The results of two ECC Galileo satellites (E14 and E18) are lacked in Figures 6–8 for the reason that their precise ephemeris data are unavailable in 5s-inteval CNES products. The SISREs of these two satellites are obviously bigger than other Galileo satellites [24], however, from Figure 13, the L1 carrier residuals of ARTK for these two satellites are near to other Galileo satellites, which show that the time-delay related broadcast ephemeris errors for E14 and E18 are also small. The time-delay related broadcast clock offset errors are neglected in [12] for ARTK, however, it should be considered according to experiment results in this study. In this study, we just provide a workable method for evaluating the variation of broadcast orbit and clock offset errors during the latency time against the selective precise products. This work does not provide an in-depth study on time variations of satellite orbit and clock offset errors. We leave this topic to future research. The GNSS signal type difference in different systems are not considered when comparing the ARTK performance among four systems in this study, because their influence on user range errors are relatively small compared with the time-delay related broadcast ephemeris and ionsphere errors in ARTK model.

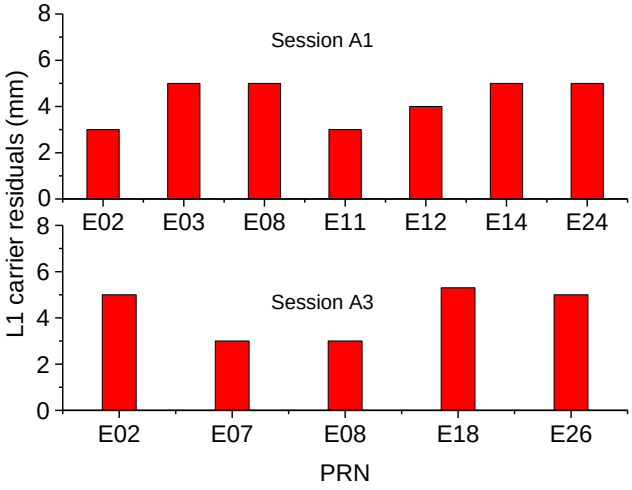

Figure 13. L1 carrier residuals of Galileo ARTK using broadcast ephemeris in Session A1 and A3 for Bs.2.

Experiment results from Sections 3.3 and 3.4 have also indicated possibility to improvement of the performance of multi-GNSS combined ARTK solutions by considering the different characteristics of broadcast ephemeris and ionosphere error variation analyzed in this study. For example, the weight of GLONASS satellites should be reduced due to their large variation of broadcast ephemeris error, and the weight of ten GPS Block IIF satellites loaded with Rb clocks can be increased relative to other GPS satellites. More precise stochastic models may be introduced in ARTK processing by taking advantages of the estimated variances for orbit, clock, and ionosphere errors as functions of time delay intervals.

5. Conclusions

Real-time kinematic (RTK) algorithms applies the double-difference technique to eliminate satellite and receiver-specific hardware delays and clock biases and effects of atmosphere and broadcast orbit errors in the code and phase measurements. A less studied problem is that the observation samples at two receivers are often asynchronous, because of different sample rates taken at reference and user receivers and the time delay for data communication between the reference and user receivers. In this contribution, the time delay related error terms in ARTK model and formulas for studying the broadcast orbit and clock offset errors and ionosphere error have been derived. Comprehensive experimental analysis has been performed to numerically show time variations of these errors and their impacts on RTK results from short-baselines. The following findings are obtained from numerical analysis:

In the asynchronous RTK mode, the degradation of position RMS precision can reach a few centimeters, but the accuracy degradation to a different degree by different systems. BDS and Galileo ARTK usually perform better than GPS and GLONASS due to the smaller variation of broadcast ephemeris error.

Based on selective precise ephemeris products, the time variation of broadcast ephemeris error is assessed. The average RMS statistics of broadcast orbit error variation over the latency of 15 s are 1.6, 9.3, 2.6, and 1.4 mm for GPS, GLONASS, BDS, and Galileo. The average RMS statistics for the variation of broadcast clock offset error are 10.6, 14.0, 6.3, and 2.6 mm for GPS, GLONASS, BDS, and Galileo, respectively. Overall, the clock offset error influence appears more serious for the ARTK model. The variation of GLONASS orbit error is most serious among four systems. From one-month long data, the average RMS statistics for 15 s latency variation of the total broadcast ephemeris error are 11.2, 16.9, 7.3 and 3.0 mm for GPS, GLONASS, BDS, and Galileo.

The performance of ARTK decreases due to the influence of ionosphere error variation. The variation of ionosphere error for some satellites over 15 s can reach a few centimeters under higher ionosphere activity sessions. In addition, compared with the other systems, BDS ARTK shows an advantage under higher ionosphere activity levels. The possible reason is that the variation of ionosphere error for five BDS GEO satellites is usually small because of their geometry structure almost staying the same.

Author Contributions: B.S. conceived the idea and designed the experiments with H.L. B.S. and Y.F. wrote the main manuscript. L.X., Z.Y. and C.Q. reviewed the paper. All components of this research were carried out under the supervision of B.S.

Funding: This work is funded by the project "Research on Real-time and High-accuracy Multi-GNSS Location Based Service Platform" (No. 2018010401011271) and the National Key Research and Development Program of China (No. 2016YFB0800405).

Acknowledgments: The authors would like to thank the Curtin University for providing open access GNSS observations.

Conflicts of Interest: The authors declare no conflict of interest.

References

1. Teunissen, P.J. The least-squares ambiguity decorrelation adjustment: a method for fast GPS integer ambiguity estimation. *J. Geod.* **1995**, *70*, 65–82. [CrossRef]
2. Zhodzishsky, M.; Vorobiev, M.; Khvalkov, A.; Ashjaee, J. Real-time kinematic (RTK) processing for dual-frequency GPS/GLONASS. In Proceedings of the ION GPS 1998, Nashville, TN, USA, 15–18 September 1998; pp. 1325–1331.
3. Edwards, S.; Cross, P.; Barnes, J.; Betaille, D. A methodology for benchmarking real time kinematic GPS. *Surv Rev.* **1999**, *35*, 163–174. [CrossRef]
4. Deng, C.; Tang, W.; Liu, J.; Shi, C. Reliable single-epoch ambiguity resolution for short baselines using combined GPS/BeiDou system. *GPS Solut.* **2014**, *18*, 375–386. [CrossRef]

5. He, H.; Li, J.; Yang, Y.; Xu, J.; Guo, H.; Wang, A. Performance assessment of single-and dual-frequency BeiDou/GPS single-epoch kinematic positioning. *GPS Solut.* **2014**, *18*, 393–403. [CrossRef]
6. Odolinski, R.; Teunissen, P.J.; Odijk, D. Combined BDS, Galileo, QZSS and GPS single-frequency RTK. *GPS Solut.* **2015**, *19*, 151–163. [CrossRef]
7. Paziewski, J.; Wielgosz, P. Assessment of GPS+ Galileo and multi-frequency Galileo single-epoch precise positioning with network corrections. *GPS Solut.* **2014**, *18*, 571–579. [CrossRef]
8. Odijk, D.; Wanninger, L. Differential Positioning. In *Springer Handbook of Global Navigation Satellite Systems*; Teunissen, P.G., Montenbruck, O., Eds.; Springer International Publishing: Cham, Switzerland, 2017; ISBN 978-3-319-42926-7.
9. Lawrence, D.G. Reference Carrier Phase Prediction for Kinematic GPS. US Patent 5,903,236, 1999.
10. Hatch, R.R.; Richard, T.S.; Yang, Y. GPS Navigation Using Successive Differences of Carrier-Phase Measurements. U.S. Patent 7,212,155, 2007.
11. Wang, H.; Ou, J.; Yuan, Y. Strategy of data processing for GPS rover and reference receivers using different sampling rates. *IEEE Trans. Geosci. Remote Sens.* **2011**, *49*, 1144–1149.
12. Zhang, L.; Lv, H.; Wang, D.; Hou, Y.; Wu, J. Asynchronous RTK precise DGNSS positioning method for deriving a low-latency high-rate output. *J. Geod.* **2015**, *89*, 641–653.
13. Lou, Y.D.; Zhang, W.X.; Wang, C.; Yao, X.G.; Shi, C.; Liu, J.N. The impact of orbital errors on the estimation of satellite clock errors and PPP. *Adv. Space Res.* **2014**, *54*, 1571–1580. [CrossRef]
14. Montenbruck, O.; Gill, E.; Kroes, E. Rapid orbit determination of LEO satellites using IGS clock and ephemeris products. *GPS Solut.* **2005**, *9*, 226–235. [CrossRef]
15. Guo, F.; Zhang, X.; Li, X.; Cai, S. Impact of sampling rate of IGS satellite clock on precise point positioning. *Geo-spat Inf.Sci.* **2010**, *13*, 150–156. [CrossRef]
16. Heng, L.; Gao, G.X.; Walter, T.; Enge, P. Statistical characterization of GPS signal-in-space errors. In Proceedings of the ION ITM 2011, San Diego, CA, USA, 24–26 January 2011; pp. 312–319.
17. Chen, L.; Jiao, W.; Huang, X.; Geng, C.; Ai, L.; Lu, L.; Hu, Z. Study on signal-in-space errors calculation method and statistical characterization of BeiDou navigation satellite system. In Proceedings of the China Satellite Navigation Conference (CSNC), Wuhan, China, 15–17 May 2013; pp. 423–434.
18. Montenbruck, O.; Steigenberger, P.; Hauschild, A. Broadcast versus precise ephemerides: a multi-GNSS perspective. *GPS Solut.* **2015**, *19*, 321–333. [CrossRef]
19. *RTCM Standard 10403.2—Differential GNSS (Global Navigation Satellite Systems) Services Version 3*; Radio Technical Commision for Maritime Services: Arlington, VA, USA, 2013.
20. Wang, J. An approach to GLONASS ambiguity resolution. *J. Geod.* **2000**, *74*, 421–430. [CrossRef]
21. Wanninger, L. Carrier-phase inter-frequency biases of GLONASS receivers. *J. Geod.* **2012**, *86*, 139–148. [CrossRef]
22. Euler, H.J.; Goad, C.C. On optimal filtering of GPS dual frequency observations without using orbit information. *Bull. Geod.* **1991**, *65*, 130–143. [CrossRef]
23. Malys, S.; Larezos, M.; Gottschalk, S.; Mobbs, S.; Winn, B.; Feess, W.; Mathon, W. The GPS accuracy improvement initiative. In Proceedings of the ION GPS, Kansas, MO, USA, 16–19 September 1997; pp. 375–384.
24. Robustelli, U.; Benassai, G.; Pugliano, G. Signal in Space Error and Ephemeris Validity Time Evaluation of Milena and Doresa Galileo Satellites. *Sensors.* **2019**, *19*, 1786. [CrossRef] [PubMed]
25. Lu, C.; Li, X.; Nilsson, T.; Ning, T.; Heinkelmann, R.; Ge, M. Real-time retrieval of precipitable water vapor from gps and beidou observations. *J. Geod.* **2015**, *89*, 843–856. [CrossRef]
26. Hadas, T.; Teferle, F.N.; Kazmierski, K.; Hordyniec, P.; Bosy, J. Optimum stochastic modeling for GNSS tropospheric delay estimation in real-time. *GPS Solut.* **2017**, *21*, 1069–1081. [CrossRef]
27. Yang, Z.; Liu, Z. Investigating the inconsistency of ionospheric ROTI indices derived from GPS modernized L2C and legacy L2 P (Y) signals at low-latitude regions. *GPS Solut* **2017**, *21*, 783–796. [CrossRef]
28. Available online: http://saegnss2.curtin.edu.au/ldc/rawdata (accessed on 26 May 2019).
29. Alber, C.; Ware, R.; Rocken, C.; Braun, J. Obtaining single path phase delays from GPS double differences. Geophys. *Res. Lett.* **2000**, *27*, 2661–2664. [CrossRef]
30. Available online: http://www2.unb.ca/gge/Resources/GPSConstellationStatus.txt (accessed on 26 May 2019).

31. Li, H.; Liao, X.; Li, B.; Yang, L. Modeling of the GPS satellite clock error and its performance evaluation in precise point positioning. *Adv. Space Res.* **2018**, *62*, 845–854. [CrossRef]
32. Van Bree, R.J.P.; Tiberius, C.C.J.M.; Hauschild, A. Real time satellite clocks in single frequency precise point positioning. In Proceedings of the ION GNSS, Savannah, GA, USA, 22–25 September 2009.